Monthly Notices
of the
ROYAL ASTRONOMICAL SOCIETY

MNRAS **438,** 3568–3576 (2014)
Advance Access publication 2014 January 28

doi:10.1093/mnras/stt2469

Electrostatic plasma instabilities driven by neutral gas flows in the solar chromosphere

G. Gogoberidze,[1,2]★ Y. Voitenko,[3] S. Poedts[4] and J. De Keyser[3]

[1]*Dipartimento di Fisica, Università della Calabria, I-87036 Rende, Italy*
[2]*Institute of Theoretical Physics, Ilia State University, Cholokashvili Ave 3/5, Tbilisi GE-0162, Georgia*
[3]*Solar–Terrestrial Centre of Excellence, Belgian Institute for Space Aeronomy, Ringlaan 3, B-1180 Brussels, Belgium*
[4]*CPA/K.U.Leuven, Celestijnenlaan 200B, B-3001 Leuven, Belgium*

Accepted 2013 December 20. Received 2013 December 18; in original form 2013 April 11

ABSTRACT

We investigate electrostatic plasma instabilities of Farley–Buneman (FB) type driven by quasi-stationary neutral gas flows in the solar chromosphere. The role of these instabilities in the chromosphere is clarified. We find that the destabilizing ion thermal effect is highly reduced by the Coulomb collisions and can be ignored for the chromospheric FB-type instabilities. In contrast, the destabilizing electron thermal effect is important and causes a significant reduction of the neutral drag velocity triggering the instability. The resulting threshold velocity is found as function of chromospheric height. Our results indicate that the FB-type instabilities are still less efficient in the global chromospheric heating than the Joule dissipation of the currents driving these instabilities. This conclusion does not exclude the possibility that the FB-type instabilities develop in the places where the cross-field currents overcome the threshold value and contribute to the heating locally. Typical length-scales of plasma density fluctuations produced by these instabilities are determined by the wavelengths of unstable modes, which are in the range 10–10^2 cm in the lower chromosphere and 10^2–10^3 cm in the upper chromosphere. These results suggest that the decimetric radio waves undergoing scattering (scintillations) by these plasma irregularities can serve as a tool for remote probing of the solar chromosphere at different heights.

Key words: Sun: chromosphere.

1 INTRODUCTION

Since it was discovered that the temperature in the solar chromosphere is much higher than that can be expected in radiative equilibrium, the mechanism of chromospheric heating is one of the main puzzles in solar physics. The first scenario for coronal and chromospheric heating was proposed by Biermann (1946) and Schwarzschild (1948), who suggested that the atmosphere of the sun is heated by acoustic waves generated in the turbulent convective zone. The theory of wave generation by turbulence was developed by Lighthill (1952). Extension of this theory to the stratified environment of the solar atmosphere showed that short-period acoustic waves are abundantly generated in the convective zone (Stein 1967). The theory predicts that the peak of the acoustic power spectrum is just below a period of one minute. Later numerical simulations (e.g. Carlsson & Stein 1992) confirmed that the total power of the generated acoustic waves is sufficient for chromospheric heating. But the measurements of acoustic flux in the chromosphere have usually failed to find sufficient energy. From the analysis of the Doppler shifts of UV lines, Bruner (1978) demonstrated that the energy flux of the acoustic waves with periods of 100 s or more is at least two orders of magnitude less than that required for the observed level of chromospheric heating. Similar results have been obtained by Mein & Schmieder (1981) from an analysis of the Doppler shifts of Ca II and Mg I lines. Recent analysis of the data obtained by *TRACE* (Fossum & Carlsson 2005) has shown that the observed intensity of high-frequency (10–50 mHz) acoustic waves was at least one order of magnitude lower than necessary for the observed chromospheric heating. In addition, instead of steepening and dissipation, the acoustic waves and pulses can form sausage solitons, propagating undamped along magnetic flux tubes (Zaqarashvili, Kukhianidze & Khodachenko 2010).

Problems with measurements of sufficient acoustic flux stimulated development of alternative models of chromospheric heating. One of the alternative scenarios (Parker 1988; Sturrock 1999) implies that impulsive nanoflares related to magnetic reconnection can be responsible for chromospheric heating. The observations (e.g. Aschwanden et al. 2000) do show numerous fast brightenings in the sun but they are not sufficiently frequent to explain the UV emission of the chromosphere. Another scenario for chromospheric heating is resistive dissipation of electric currents (Rabin & Moore 1984;

★ E-mail: grigol_gogoberidze@iliauni.edu.ge

Goodman 2004). Recent analysis of three-dimensional vector currents observed in a sunspot has shown that the observed currents are not sufficient to be responsible for the observed amount of heating (Socas-Navarro 2007).

Recently, it has been supposed that a convective motion-driven Farley–Buneman instability (FBI; Buneman 1963; Farley 1963) can significantly contribute to chromospheric heating (Liperovsky et al. 2000; Fontenla 2005; Fontenla, Peterson & Harder 2008). The FBI is known to be responsible for the formation of plasma irregularities in the Earth's ionospheric E-region (Schunk & Nagy 2000). The interplay of the background electric and magnetic fields at the altitudes, where electrons are strongly magnetized produces currents that drive the instability. In a similar way, if the electrons are strongly magnetized, the drag of the ions by neutrals causes the instability. The simultaneously observed electron heating was attributed to the parallel electric fields in waves (Dimant & Milikh 2003; Milikh & Dimant 2003). Gogoberidze et al. (2009) extended analysis of the FBI in the solar chromosphere conditions by taking into account the finite ion magnetization and Coulomb collisions. This study suggested that the FBI is not a dominant factor in the global chromospheric heating. However, local strong cross-field currents can drive FBI producing small-scale (0.1–3m) density irregularities and contributing to the chromospheric heating locally. Pandey & Wardle (2013) accounted for the flow inhomogeneity (flow shears) and found an electromagnetic magnetohydrodynamic-like instability generated at larger scales. These irregularities can cause scintillations of radio waves at similar length-scales and provide a tool for chromospheric remote sensing. It has to be noted that Gogoberidze et al. (2009) did not take into account effects of the electron heating related to the presence of parallel electric fields in the waves. As showed theoretically by Dimant & Milikh (2003) and confirmed by recent particle in cell simulations (Oppenheim & Dimant 2013), this effect can significantly increase the electron heating. Importance of this mechanism for the solar chromosphere requires an additional analysis and is beyond the scope of this paper.

It is also known that electron and ion thermal effects can strongly affect small-scale E-region instabilities. The electron thermal effects lead to a considerable modification of the FBI (mainly by the electron Pedersen conductivity via perturbed Joule heating), and Dimant & Sudan (1995) have given the modified FBI a new name: electron Pedersen conductivity instability. Later on, this instability was studied in more detail by Dimant & Sudan (1997) and Robinson (1998). The ion thermal effects also modify FBI significantly and make it possible in a wider altitude range as compared to the predictions of adiabatic and isothermal FBI models (Dimant & Oppenheim 2004).

Here, we study small-scale electrostatic instabilities of the FB type in the partially ionized plasma of the solar chromosphere taking into consideration ion and electron thermal effects, electron and ion viscosity and Coulomb collisions. As it has been demonstrated by Gogoberidze et al. (2009), contrary to the ionospheric case, the Coulomb collisions of electrons and ions cannot be ignored in the chromosphere because of the relatively high degree of ionization (10^{-2}–10^{-4}). In this paper, we find another difference with the ionosphere: the destabilizing influence of ion thermal effects is highly reduced in the chromosphere by Coulomb collisions and can be neglected. But electron thermal effects appeared to be important, especially in the middle and upper chromosphere, where they reduce the threshold value of the relative electron/ion velocity (current velocity). We determine various characteristic length-scales as well as the value of the threshold relative velocity of electrons and ions necessary to trigger the electrostatic instability as a function of chromospheric height in the framework of the semi-empirical chromospheric model SRPM 306 (Fontenla, Balasubramaniam & Harder 2007). We confirm our previous conclusion that FB-type electrostatic instabilities cannot be responsible for the chromospheric heating at global length-scales. However, such instabilities can be generated locally in the places of sufficiently strong currents and can create small-scale plasma irregularities.

The paper is organized as follows. The general formalism is presented in Section 2. The FBI and the ion thermal instability are studied in Section 3. The electron thermal instability is discussed in Section 4. Different length-scales of the chromosphere important for the development of electrostatic instabilities are studied in Section 5. Conclusions are given in Section 6.

2 GENERAL FORMALISM

We use a standard modal analysis for linear perturbations in partially ionized plasmas with neutral flows taking into account Coulomb collisions, ion and electron viscosity, and thermal effects. The dynamics of electrons, one species of singly charged ions and neutral hydrogen in the solar chromosphere for imposed electric ($\boldsymbol{E}$) and magnetic ($\boldsymbol{B}$) fields is governed by the continuity, Euler and heat transfer equations

$$\frac{\mathrm{d}_\alpha n_\alpha}{\mathrm{d}t} + n_\alpha \nabla \cdot \boldsymbol{V}_\alpha = 0, \tag{1}$$

$$m_\mathrm{e}\frac{\mathrm{d}_\mathrm{e}\boldsymbol{V}_\mathrm{e}}{\mathrm{d}t} = -e\left(\boldsymbol{E} + \frac{\boldsymbol{V}_\mathrm{e}\times\boldsymbol{B}}{c}\right) - \frac{\nabla(n_\mathrm{e}\mathcal{K}T_\mathrm{e})}{n_\mathrm{e}} - m_\mathrm{e}\nu_\mathrm{ei}(\boldsymbol{V}_\mathrm{e}-\boldsymbol{V}_\mathrm{i}) - m_\mathrm{e}\nu_\mathrm{en}(\boldsymbol{V}_\mathrm{e}-\boldsymbol{V}_\mathrm{n}) + m_\mathrm{e}\eta_\mathrm{e}\nabla^2\boldsymbol{V}_\mathrm{e}, \tag{2}$$

$$m_\mathrm{i}\frac{\mathrm{d}_\mathrm{i}\boldsymbol{V}_\mathrm{i}}{\mathrm{d}t} = e\left(\boldsymbol{E} + \frac{\boldsymbol{V}_\mathrm{i}\times\boldsymbol{B}}{c}\right) - \frac{\nabla(n_\mathrm{i}\mathcal{K}T_\mathrm{i})}{n_\mathrm{i}} - m_\mathrm{e}\nu_\mathrm{ei}(\boldsymbol{V}_\mathrm{i}-\boldsymbol{V}_\mathrm{e}) - \mu_\mathrm{ni}m_\mathrm{i}\nu_\mathrm{in}(\boldsymbol{V}_\mathrm{i}-\boldsymbol{V}_\mathrm{n}) + m_\mathrm{i}\eta_\mathrm{i}\nabla^2\boldsymbol{V}_\mathrm{i}, \tag{3}$$

$$n_\mathrm{e}^{2/3}\frac{\mathrm{d}_\mathrm{e}(T_\mathrm{e}n_\mathrm{e}^{-2/3})}{\mathrm{d}t} = \frac{2}{3}\varepsilon_\mathrm{e}\mu_\mathrm{ne}m_\mathrm{e}\nu_\mathrm{en}(\boldsymbol{V}_\mathrm{e}-\boldsymbol{V}_\mathrm{n})^2 - 2\mu_\mathrm{en}\nu_\mathrm{en}(1+\rho_\mathrm{en})(T_\mathrm{e}-T_\mathrm{n}) + \frac{2}{3}\mu_\mathrm{ie}m_\mathrm{e}\nu_\mathrm{ei} \times (\boldsymbol{V}_\mathrm{e}-\boldsymbol{V}_\mathrm{i})^2 - 2\mu_\mathrm{ei}\nu_\mathrm{ei}(T_\mathrm{e}-T_\mathrm{i}) + \frac{\chi_\mathrm{e}}{n_\mathrm{e}}\nabla^2 T_\mathrm{e}, \tag{4}$$

$$n_\mathrm{i}^{2/3}\frac{\mathrm{d}_\mathrm{i}(T_\mathrm{i}n_\mathrm{i}^{-2/3})}{\mathrm{d}t} = \frac{2}{3}\varepsilon_\mathrm{i}\mu_\mathrm{ni}m_\mathrm{i}\nu_\mathrm{in}(\boldsymbol{V}_\mathrm{i}-\boldsymbol{V}_\mathrm{n})^2 - 2\mu_\mathrm{ni}\nu_\mathrm{in}(T_\mathrm{i}-T_\mathrm{n}) + \frac{2}{3}\mu_\mathrm{ei}m_\mathrm{i}\nu_\mathrm{ei}(\boldsymbol{V}_\mathrm{e}-\boldsymbol{V}_\mathrm{i})^2 - 2\mu_\mathrm{ei}\nu_\mathrm{ei}(T_\mathrm{i}-T_\mathrm{e}) + \frac{\chi_\mathrm{i}}{n_\mathrm{i}}\nabla^2 T_\mathrm{i}. \tag{5}$$

Here, $\alpha = \mathrm{e}, \mathrm{i}$ denotes electrons or ions; n denotes neutrals; n_α is the number density, $\boldsymbol{V}_\alpha$ is the averaged drift velocity; m_α is the mass; T_α is the temperature; $\nu_{\alpha\beta}$ is the elastic collision frequency; η_α is the kinematic viscosity; χ_α is the thermal conductivity; $\mu_{\alpha\beta} = m_\alpha/(m_\alpha + m_\beta)$ is the mass-reducing factor, such that $2\mu_{\alpha\beta}$ is the energy fraction lost by a particle of α species during one elastic collision with a particle of β species; c is the speed of light; $\mathcal{K}$ is the Boltzmann constant and $\mathrm{d}_\alpha/\mathrm{d}t$ denotes the convective derivative.

$\varepsilon_{e,i}$ are dimensionless parameters which will be discussed below. The relative efficiency of inelastic/elastic collisions in the electron thermal balance is $\rho_{en} = \bar{\nu}_{en}/(3\mu_{en}\nu_{en})$, where $\bar{\nu}_{en}$ is the inelastic $e-n$ collisional frequency.

Equations (1)–(5) are similar to the so-called 5-moment transport equations (Schunk & Nagy 2000) which are often used when studying instabilities in the E-region of the Earth's ionosphere. The principal difference between the 5-moment approach and our study is that, as it was mentioned in the introduction, the ionization degree in the chromosphere is much higher than in the E-region and consequently Coulomb collisions are not ignored in the set of equations (1)–(5). We account for inelastic $e-n$ collisions (Robinson 1998) in the electron energy balance (4) (term proportional to ρ_{en}). We will come back to this last issue in the discussion section.

The right-hand side of equations (4) and (5) describe the balance between frictional heating (two positive terms) and collisional cooling (two negative terms). Without these effects, the temperature fluctuations would be adiabatic ($T_\alpha \sim n_\alpha^{\gamma-1}$ with $\gamma = 5/3$). In the case of elastic collisions, we have $\mu_{ei} = m_e/(m_e + m_i) \approx m_e/m_i$, and $\mu_{ni} \approx m_p/(m_p + m_i)$.

In the upper chromosphere, the charged particles are mainly protons (and therefore $\mu_{ni} = 1/2$), whereas at lower attitudes heavy ions dominate the positive charge. Because of this reason, we do not specify the type of ions and the obtained results will be suitable for studying both upper and lower chromosphere. This circumstance leads to other distinctions from the similar ionospheric analysis. Namely for lower chromosphere we have $\mu_{ni} \approx m_p/m_i$ and the influence of the ion–neutral friction on ion dynamics is reduced by factor m_p/m_i in comparison to the case of equal ion/neutral masses.

The frictional heating terms in equations (4) and (5) include additional factors $\varepsilon_{e,i}$ that account for possible effects of enhanced wave heating. Ionospheric observations shows that the typical value of ε_e varies between 10 and 30 in the middle ionosphere (Robinson 1998; Dimant & Milikh 2003), whereas no ion heating is usually observed (i.e. $\varepsilon_i = 1$ in the ionosphere). Chromospheric factors driving waves unstable appeared to be quite different from the ionospheric ones, and the enhanced ion heating by the waves may occur in the chromosphere as well as the enhanced electron heating. We would like to account for this possibility by putting $\varepsilon_i \neq 1$, and for simplicity we will use the single heating parameter $\varepsilon = \varepsilon_e = \varepsilon_i$.

For collision frequencies, we use the following expressions (Braginskii 1965):

$$\nu_{ei} = \frac{4(2\pi)^{1/2} e^4 n_e \Lambda}{3 m_e^{1/2} (\mathcal{K} T_e)^{3/2}}, \tag{6}$$

$$\nu_{en} = \sigma_{en} n_n \sqrt{\frac{\mathcal{K} T_e}{m_e}}, \tag{7}$$

$$\nu_{in} = \nu_{pn} = \sigma_{in} n_n \sqrt{\frac{\mathcal{K} T_p}{m_p}}, \tag{8}$$

where Λ is the Coulomb logarithm. From the former equation, we see that regardless of the mass of dominant ion species, $\nu_{ei} = \nu_{ep}$ for singly charged ions.

For the electron–neutral and ion–neutral collisions, we assume a simple model with constant cross-sections $\sigma_{en} = 3.0 \times 10^{-15}\,\mathrm{cm}^2$ (Bedersen & Kieffer 1971) and $\sigma_{in} = 2.8 \times 10^{-14}\,\mathrm{cm}^2$ (Krstic & Schultz 1999) that are typical for the middle chromosphere with particles energies $\sim 0.5-1.0$ eV. In principle, σ_{en} and σ_{in} are not constant but depend on the particles energies. For example, the neutral atom polarization results in the $\sigma_{sn} \sim 1/V_s$ dependence making the collisional frequency independent of the particle energy. With this model, our results would even more emphasize the effects of Coulomb collisions on FBI in the upper chromosphere. However, because of the other kinds of collisions with neutrals, the atom polarization model underestimates the electron and ion collisions with the neutrals. Since these other kinds of collisions with neutrals are not well studied in the chromospheric conditions, we use the model with constant cross-sections, which artificially enhances ν_{en} and ν_{in} at larger heights.

Estimation of inelastic electron–hydrogen collisional frequency $\bar{\nu}_{en}$ is rather involved and sensitive to the electron temperature and velocity distribution in the superthermal tail. Taking into account two main excitation levels of hydrogen atoms and using formulae given by Johnson (1972), we estimate that ρ_{en} vary from 0.1 in the lower chromosphere to about 1 in the upper chromosphere. We will keep ρ_{en} in derivations, but will not analyse its influence separately (see Discussion).

We assume that the system is penetrated by a uniform magnetic field $\boldsymbol{B}$ and that neutrals have background velocity $\boldsymbol{V}_n \perp \boldsymbol{B}$. Then, equation (2) and (3) give for the background flow of electrons and ions

$$\kappa \boldsymbol{V}_i \times \boldsymbol{b} - (\alpha N + \mu_{ni})\boldsymbol{V}_i + \alpha N \boldsymbol{V}_e + \mu_{ni}\boldsymbol{V}_n = 0, \tag{9}$$

$$-\kappa \boldsymbol{V}_e \times \boldsymbol{b} - \alpha(N+1)\boldsymbol{V}_e + \alpha N \boldsymbol{V}_i + \alpha \boldsymbol{V}_n = 0. \tag{10}$$

Here, $\kappa = \omega_{cp}/\nu_{pn}$ is the proton magnetization, $\boldsymbol{b} = \boldsymbol{B}/B$ is the unit vector along the mean magnetic field direction, $\psi = \nu_{en}\nu_{in}/\omega_{cp}\omega_{ce}$, $\omega_{c\alpha} \equiv eB/m_\alpha c$ is the cyclotron frequency, $\alpha = \psi\kappa^2 = m_e\nu_{en}/m_p\nu_{pn} \approx 2.6 \times 10^{-3}$ and $N = \nu_{ei}/\nu_{en}$ is the ratio of the Coulomb and electron–neutral collision frequencies.

Multiplying equations (9) and (10) by $\boldsymbol{b}$ and excluding $\boldsymbol{V}_i \times \boldsymbol{b}$ and $\boldsymbol{V}_e \times \boldsymbol{b}$, we obtain

$$\left[\frac{\kappa^2}{\mu_1}(N+1) + \alpha N + \mu_{ni}\right]\boldsymbol{V}_i - N\left[\frac{\kappa^2}{\mu_1} + \alpha\right]\boldsymbol{V}_e = \kappa \boldsymbol{V}_n \times \boldsymbol{b} + \mu_{ni}\boldsymbol{V}_n, \tag{11}$$

$$N\left[\frac{\kappa^2}{\mu_1} + \alpha\right]\boldsymbol{V}_i - \left[\frac{\kappa^2(\alpha N + \mu_{ni})}{\alpha\mu_1} + \alpha(1+N)\right]\boldsymbol{V}_e = \kappa \boldsymbol{V}_n \times \boldsymbol{b} - \alpha \boldsymbol{V}_n. \tag{12}$$

Here, $\mu_1 = \alpha N + \mu_{ni}(1+N) \approx \mu_{ni}(1+N)$.

Using equations (11) and (12) one can readily derive expressions for $\boldsymbol{V}_i$ and $\boldsymbol{V}_i$, but exact relations are too complicated. The dependence of the proton magnetization κ and N on height based on the semi-empirical chromospheric model SRMP 306 (Fontenla et al. 2007) is shown in Figs 1 and 2, respectively. Detailed analysis of these data is presented in the next section. Here, we note that, as it can be seen from Fig. 2, for all chromospheric heights $\alpha N \ll 1$. Also, from the data shown in Figs 1 and 2, one can find that $\kappa^2/\mu_1 \gg \alpha$ in the chromosphere except for very low altitudes $h < 600$ km. In this paper, we are mostly interested in higher altitudes where the Coulomb collisional effects are important for FBI. In the limit $\alpha N \ll 1$ and $\alpha\mu_1/\kappa^2 \ll 1$, we obtain the ion and electron background velocities

$$\boldsymbol{V}_i \approx \frac{\mu_{ni}}{\kappa^2 + \mu_{ni}^2}\left[\mu_{ni}\boldsymbol{V}_n + \kappa \boldsymbol{V}_n \times \boldsymbol{b}\right], \tag{13}$$

$$\boldsymbol{V}_e \approx \alpha\mu_{ni}\frac{N\kappa^2 + \alpha\mu_{ni}(1+N)}{\kappa^2(\kappa^2 + \mu_{ni}^2)}\boldsymbol{V}_n - \alpha\frac{\kappa^2 + \mu_{ni}^2(1+N)}{\kappa(\kappa^2 + \mu_{ni}^2)}\boldsymbol{V}_n \times \boldsymbol{b}. \tag{14}$$

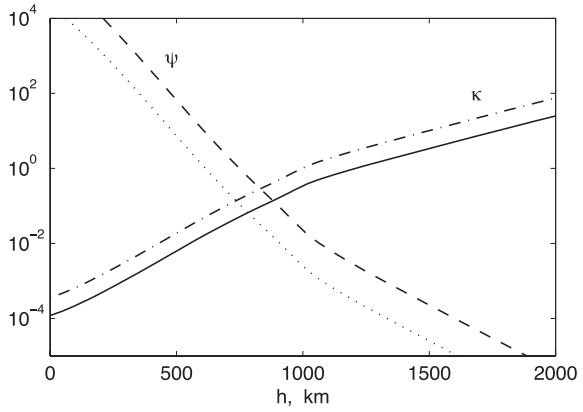

Figure 1. Proton magnetization κ_p in the chromosphere for $B = 30$ G (solid line) and $B = 90$ G (dash–dotted line), and ψ for $B = 30$ G (dashed line) and $B = 90$ G (dotted line).

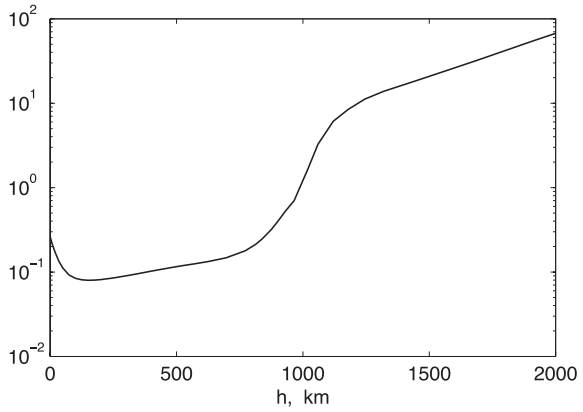

Figure 2. The ratio N of the Coulomb to electron–neutral collision frequencies as a function of height.

In the considered limit, $\alpha \ll 1$ and $\alpha N \ll 1$, the current velocity $\boldsymbol{U}_0 = \boldsymbol{V}_\mathrm{i} - \boldsymbol{V}_\mathrm{e} \approx \boldsymbol{V}_\mathrm{i}$.

On the background given by equations (13) and (14) and corresponding solutions for ion and electron temperatures in the subsequent sections, we consider different linear electrostatic perturbations propagating in the plane perpendicular to the background magnetic field. To simplify further analysis, we make two assumptions which are standard in the study of low-frequency perturbations. First, we assume quasi-neutrality ($n_\mathrm{e} \approx n_\mathrm{i} = n$). This condition is valid when characteristic frequency of perturbations is much less than ion plasma frequency. Secondly, we treat electrons as inertialess. The latter assumption implies that the characteristic time-scale of the perturbations is much greater than electron cyclotron and plasma time-scales. Both ion thermal and current-driven instabilities occur at ion–neutral collision time-scale, which for typical chromospheric parameters is much greater than all characteristic time-scales mentioned above.

In the analysis below, we ignore perturbations of the neutral component. Such a treatment is valid in weakly ionized plasma for relatively high-frequency perturbations. Comparing inertial and ion drag terms in the Euler equation for neutrals, we obtain that perturbations of the neutral component can be safely neglected if

$$\omega \gg \frac{n_\mathrm{e}}{n_\mathrm{n}} \nu_\mathrm{in}. \tag{15}$$

And finally, as is usually done in the E-layer research, we consider the ion and electron temperature perturbations separately. Due to the relatively high electron concentration in the chromosphere we do not ignore Coulomb collisions. In the general case, perturbations of the ion temperature can cause perturbations of the electron temperature. But due to the large ions/electron mass ratio, Coulomb collisions are inefficient in the heat transfer between electrons and ions. Mathematically, this is manifested by the $\mu_\mathrm{ei} \sim m_\mathrm{e}/m_\mathrm{i}$ multiplier in the last but one term of equation (5). Comparing this term with the left-hand side of equation (5) shows that the thermal perturbations of ions and electrons can be treated separately if

$$\omega \gg \frac{m_\mathrm{e}}{m_\mathrm{i}} \nu_\mathrm{ei}. \tag{16}$$

In this context, it should be also noted that electron thermal effects in the ionospheric E-layer are important for relatively low altitudes (Schunk & Nagy 2000), where ion magnetization is weak, whereas ion thermal effects become important with strong ion magnetization.

3 FBI AND ION THERMAL EFFECTS

Let as introduce dimensionless perturbations of electric potential, number density and temperature for the α species:

$$\bar{\phi}_\alpha = \frac{e\boldsymbol{k}\cdot\boldsymbol{E}'}{\mathcal{K}T_\alpha k^2}, \quad \bar{n} = \frac{n'}{n}, \quad \bar{\tau}_\alpha = \frac{T'_\alpha}{T_\alpha}, \tag{17}$$

where primed variables stand for linear perturbations in the Fourier space and wave vector $k \perp b$ (here, we considered only two-dimensional perturbations with wave vectors perpendicular to the background magnetic field).

Then, linearizing equations (1)–(5), dropping viscosity and thermal conductivity effects (these effects will be studied in the following sections), setting for simplicity $\varepsilon = 1$ and setting $T'_\mathrm{e} = 0$, the Euler equation for the ions gives

$$\left(1 + \alpha^* N - \frac{i\Omega}{\nu^*_\mathrm{in}}\right)\boldsymbol{v}'_\mathrm{i} = -i\boldsymbol{k}\frac{u^2_{T\mathrm{i}}}{\nu^*_\mathrm{in}}(\bar{\phi}_\mathrm{i} + \bar{n} + \bar{\tau}_\mathrm{i}) + \kappa^*\boldsymbol{v}'_\mathrm{i}\times\boldsymbol{b} + \alpha^* N\boldsymbol{v}'_\mathrm{e}, \tag{18}$$

where $\Omega = \omega - \boldsymbol{k}\cdot\boldsymbol{V}_\mathrm{i}$ is the frequency in the ion frame, $\nu^*_\mathrm{in} = \mu_\mathrm{ni}\nu_\mathrm{in}$ is the reduced ion–neutral collisional frequency, $\kappa^* = \kappa/\mu_\mathrm{in}$, $\alpha^* = \alpha/\mu_\mathrm{in}$ and $u_{T\mathrm{i}} = (T_\mathrm{i}/m_\mathrm{i})^{1/2}$ is the ion thermal velocity.

Similarly, the linearized Euler equation for the electrons (which we treat inertialess) gives

$$(1+N)\,\boldsymbol{v}'_\mathrm{e} = i\boldsymbol{k}\frac{u^2_{T\mathrm{i}}}{\alpha\nu^*_\mathrm{in}}\left(\bar{\phi}_\mathrm{i} - \frac{\gamma T_\mathrm{e}}{T_\mathrm{i}}\bar{n}\right) - \frac{\kappa}{\alpha}\boldsymbol{v}'_\mathrm{e}\times\boldsymbol{b} + N\boldsymbol{v}'_\mathrm{i}. \tag{19}$$

As discussed earlier, we study evolution of perturbations in the limits $\alpha \ll 1$ and $\alpha N \ll 1$ that are fulfilled in the entire chromosphere. In addition, here we assume also $\alpha N/\kappa^2 \ll 1$. This condition is valid everywhere except for very low chromospheric heights, where the influence of Coulomb collisions on FBI is negligible anyway (Gogoberidze et al. 2009). Solving equations (18) and (19) for perturbed velocities and keeping only leading-order terms with respect to the small parameters α, αN and $\alpha N/\kappa^2$, we obtain

$$\boldsymbol{v}'_\mathrm{i} = -i\left(\frac{u^2_{T\mathrm{i}}}{\nu^*_\mathrm{in}}\right)\frac{\left(1 - i\Omega/\nu^*_\mathrm{in}\right)\boldsymbol{k} + \kappa'\boldsymbol{k}\times\boldsymbol{b}}{\left(1 - i\Omega/\nu^*_\mathrm{in}\right)^2 + \kappa'^2}(\bar{\phi}_\mathrm{i} + \bar{n} + \bar{\tau}_\mathrm{i}), \tag{20}$$

$$\boldsymbol{v}'_\mathrm{e} = i\boldsymbol{k}\psi\frac{u^2_{T\mathrm{i}}}{\nu^*_\mathrm{in}}\left[(1+N)\left(\bar{\phi}_\mathrm{i} - \frac{\gamma T_\mathrm{e}}{T_\mathrm{i}}\bar{n}\right) - \frac{N\kappa'^2(\bar{\phi}_\mathrm{i} + \bar{n} + \bar{\tau}_\mathrm{i})}{(1 - i\Omega/\nu^*_\mathrm{in})^2 + \kappa^{*2}}\right] + \boldsymbol{Q}. \tag{21}$$

Here, $\boldsymbol{Q}$ stands for the terms proportional to $\boldsymbol{k}\times\boldsymbol{b}$, which do not contribute to the dispersion relation [it is eliminated by the scalar product $\boldsymbol{k}\cdot\boldsymbol{v}_{\rm e}'$ in equation (25) below].

From equation (20), it follows that, in the lowest order with respect to the small parameters α, αN and $\alpha N/\kappa^2$, the perturbed ion velocity is not affected by the Coulomb collisions with electrons. Physically, this means that the force balance for the ion fluctuations is dominated by the ion–neutral rather than the ion–electron collisions. In the leading order with respect to small α, αN and $\alpha N/\kappa^2$, the perturbed equation (5) reduces to

$$\left(\frac{\Omega}{\nu_{\rm in}^*}+i\zeta\right)\bar{\tau}_{\rm i}-\frac{2\Omega}{3\nu_{\rm in}^*}\bar{n}=\frac{4i\mu_{\rm ni}}{3u_{T{\rm i}}^2}\boldsymbol{v}_{\rm i}'\cdot(\boldsymbol{V}_{\rm i}-\boldsymbol{V}_{\rm n}), \tag{22}$$

where $\zeta=2\mu_{\rm ni}+\nu_{\rm ep}/\nu_{\rm in}^*$.

From the ion continuity equation, using equations (13) and (20), we obtain

$$\boldsymbol{v}_{\rm i}'\cdot(\boldsymbol{V}_{\rm i}-\boldsymbol{V}_{\rm n})=\frac{\Omega\kappa'\bar{n}}{k^2(1-i\Omega/\nu_{\rm in}^*)}\times\left[(1-i\Omega/\nu_{\rm in}^*)\boldsymbol{k}\cdot(\boldsymbol{U}_0\times\boldsymbol{b})+\kappa'(\boldsymbol{k}\cdot\boldsymbol{U}_0)\right]. \tag{23}$$

Substituting this into equation (22), we obtain the relation between the temperature and density perturbations $\bar{\tau}_{\rm i}$ and $\bar{n}$:

$$\frac{3kU_0}{2\Omega}\left(1-i\frac{\Omega}{\nu_{\rm in}^*}\right)\left(\zeta-i\frac{\Omega}{\nu_{\rm in}^*}\right)\bar{\tau}_{\rm i}=\left[\frac{2\mu_{\rm ni}\kappa^2U_0^2\cos\theta}{u_{T{\rm i}}^2}+\left(1-i\frac{\Omega}{\nu_{\rm in}^*}\right)\left(\frac{2\mu_{\rm ni}\kappa^2U_0^2\sin\theta}{u_{T{\rm i}}^2}-i\frac{kU_0}{\nu_{\rm in}^*}\right)\right]\bar{n}, \tag{24}$$

where θ is the angle between $\boldsymbol{U}_0$ and $\boldsymbol{k}$.

To obtain the second independent relation between $\bar{\tau}_{\rm i}$ and $\bar{n}$, we use the electron continuity equation

$$(\Omega+\boldsymbol{k}\cdot\boldsymbol{U}_0)\bar{n}=\boldsymbol{k}\cdot\boldsymbol{v}_{\rm e}'. \tag{25}$$

Substituting equation (21) in this equation gives

$$-i\frac{k^2u_{T{\rm i}}^2}{\nu_{\rm in}^{*2}}\bar{\tau}_{\rm i}=\left[\frac{\Omega+\boldsymbol{k}\cdot\boldsymbol{U}_0}{\bar{\psi}\nu_{\rm in}^*}+i\frac{k^2c_s^2}{\nu_{\rm in}^{*2}}+\frac{\Omega}{\nu_{\rm in}^*}\frac{(1-i\Omega/\nu_{\rm in}^*)^2+\kappa^2/(1+N)}{1-i\Omega/\nu_{\rm in}^*}\right]\bar{n}, \tag{26}$$

where $c_s=[\mathcal{K}(T_{\rm i}+T_{\rm e})/m_{\rm i}]^{1/2}$ is the isothermal sound speed and $\bar{\psi}=\psi(1+N)$. Note that in the absence of thermal effects, $\bar{\tau}_{\rm i}=0$, the expression in the square brackets on the left-hand side of equation (26) represents the dispersion relation for isothermal electrostatic perturbations in weakly ionized plasmas studied by Gogoberidze et al. (2009).

By means of equations (24) and (26), which represent two independent relations between $\bar{\tau}_{\rm i}$ and $\bar{n}$, one can readily derive the dispersion relation. A simple analytical solution of the dispersion equation can be obtained in the long-wavelength low-frequency limit

$$|\Omega|,\ kU_0\ll\nu_{\rm in}^*. \tag{27}$$

Eliminating τ from equations (24) and (26), and keeping first-order terms in small parameters $|\Omega|/\nu_{\rm in}^*$ and $kU_0/\nu_{\rm in}^*$, we obtain the real part of frequency

$$\Omega_r=-\frac{\boldsymbol{k}\cdot\boldsymbol{U}_0}{1+\bar{\psi}}. \tag{28}$$

Analysis of the second-order terms yields the following expression for the growth rate

$$\gamma=\frac{\bar{\psi}k^2U_0^2}{\nu_{\rm in}^*(1+\bar{\psi})}\left[\frac{\left(1-\frac{\kappa^2}{1+N}\right)\cos^2\theta}{(1+\bar{\psi})^2}-\frac{c_s^2}{U_0^2}+\frac{4\mu_{\rm ni}}{3\zeta}\frac{\kappa\cos\theta(\kappa\cos\theta+\sin\theta)}{1+\bar{\psi}}\right]. \tag{29}$$

Equations (28) and (29) represent solution for the frequency and the growth rate in the lowest order with respect to the small parameters $\alpha, \alpha N$ and $\alpha N/\kappa^2$. Equations (28) and (29) generalize equations (29) and (30) from Dimant & Oppenheim (2004) by including Coulomb collisions and allowing for different masses of the colliding ions and neutrals.

The first term in the square brackets of equation (29) drives the FBI, while the last term drives the ion thermal instability. If Coulomb collisions are ignored ($N=0$), then the driving term reduces to the well-known result by Fejer, Providakes & Farley (1984), which implies that, regardless of the neutral drag velocity, the FBI cannot occur if the proton magnetization $\kappa>1$. The dependence of the proton magnetization κ on height in the chromosphere based on the semi-empirical chromospheric model SRPM 306 (Fontenla et al. 2007) is shown in Fig. 1 for $B=30$ G (solid line) and $B=90$ G (dash–dotted line), and ψ for $B=30$ G (dashed line) and $B=90$ G (dotted line). It is seen that the proton magnetization exceeds unity in the upper chromosphere and the standard FBI theory predicts its stability there. In contrast, as was shown by Gogoberidze et al. (2009), the Coulomb collisions make FBI possible even if ions are relatively highly magnetized [the effect of reduced magnetization $\sim\kappa^2/(1+N)$ in the numerator]. Detailed analysis shows that the effect related to the Coulomb collisions makes the FBI possible for chromospheric heights from ∼1000 to ∼1400 km (fig. 2 by Gogoberidze et al. 2009).

The dependence of $N=\nu_{\rm ep}/\nu_{\rm en}$ on the height for the model SRPM 306 is presented in Fig. 2. It is seen that Coulomb collisions become dominant at heights $h>1000$ km and hence the development of FBI is facilitated in the upper chromosphere (Gogoberidze et al. 2009).

If ion thermal effects are ignored, then the most unstable mode has $\theta=0$ and the threshold value of the current velocity necessary to trigger the FBI is given by

$$U_0^{\rm cr}=c_s(1+\bar{\psi})\left(1-\frac{\kappa^2}{1+N}\right)^{-1/2}. \tag{30}$$

Using the SRPM 306 model, Gogoberidze et al. (2009) found that the minimum value of $U_0^{\rm cr}$ occurs at chromospheric height of 850 km and is about 2 km s^{-1}, which corresponds to the current $J_0\sim2.4\times10^6$ statampere cm^{-2}. According to recent observations, the typical values of currents at length-scales ∼100 km and longer are much smaller, $\sim5\times10^4$ statampere cm^{-2} (Socas-Navarro 2007). In principle, it is possible that stronger currents exist locally at smaller scales, but in this case the heat produced by the ion–neutral friction will be at least one order of magnitude larger than the energy required to sustain the radiative losses in the chromosphere. Consequently, Gogoberidze et al. (2009) concluded the FBI cannot be responsible for chromospheric heating.

The ion thermal driving described by the last term in square brackets of equation (29) becomes important for relatively high chromospheric altitudes where the ion magnetization is strong. Analysis of

equation (29) shows that the most unstable mode propagates at the angle θ_{IT},

$$\tan\theta_{IT} = 2\kappa(1+\bar{\psi})\bar{\mu}\left[3-\kappa^2\left(\frac{3}{1+N}-2\eta\right)\right]^{-1}. \quad (31)$$

Here,

$$\bar{\mu}_{\rm pi} = \frac{2\mu_{\rm pi}}{\zeta} = \left(1+\frac{m_{\rm i}+m_{\rm p}}{2m_{\rm p}}\frac{\nu_{\rm en}}{\nu_{\rm in}}N\right)^{-1}. \quad (32)$$

For protons and heavy ions with $m_{\rm i} = 30m_{\rm p}$,

$$\bar{\mu}_{\rm pp} = \frac{1}{1+4.59N}, \quad \bar{\mu}_{\rm pi} = \frac{1}{1+71.2N}. \quad (33)$$

Using the data presented in Fig. 1, we conclude that both in the lower chromosphere (where positive charges are dominated by heavy ions) and in the upper chromosphere, the Coulomb collisions strongly reduce the ion thermal effects and make them negligible in the chromospheric conditions.

4 ELECTRON THERMAL EFFECTS

As is mentioned above, the electron thermal effects are important at relatively low altitudes, where ion magnetization is still weak. Therefore, we treat the ions as unmagnetized, whereas the electrons are assumed to be strongly magnetized, in which case $\boldsymbol{V}_{\rm i} \approx \boldsymbol{U}_0 \approx \boldsymbol{V}_{\rm n}$. Manipulations with the Euler equation for electrons under the condition $\omega_{ce} \gg \nu_{\rm en}$ yield

$$\boldsymbol{v}'_{\rm e} = \frac{\omega\bar{n}}{k^2}\left(\boldsymbol{k} - \frac{\omega_{ce}}{\nu_{\rm en}(1+N)+\eta_{\rm e}k^2}\boldsymbol{k}\times\boldsymbol{b}\right). \quad (34)$$

From the Euler equation for ions and from the continuity equation, dropping the terms of order $\psi\kappa^2 \sim 2.6\times10^{-3}$ we have

$$\boldsymbol{v}'_{\rm i} = -i\frac{\boldsymbol{k}u_{T\rm i}^2}{\nu^*_{\rm in}(1+\xi-i\Omega/\nu^*_{\rm in})}\left(\bar{n}+\frac{T_{\rm e}}{T_{\rm i}}\bar{\phi}_{\rm e}\right) = \frac{\boldsymbol{k}}{k^2}\Omega\bar{n}, \quad (35)$$

where $\xi = k^2\eta_{\rm i}/\nu^*_{\rm in}$. Substituting equations (34) and (35) into the perturbed heat balance equation for electrons, and using condition $\omega_{ce} \gg \nu_{\rm en}$, we obtain

$$\left(i - 2\omega_{ce}\varepsilon\frac{(\boldsymbol{k}\times\boldsymbol{b})\cdot\boldsymbol{U}_0}{g_{\rm en}k^2u_{T\rm e}^2} - \varepsilon\frac{2\nu_{\rm en}N\boldsymbol{k}\cdot\boldsymbol{U}_0}{\omega k^2u_{T\rm e}^2}\right)\bar{n}$$
$$= \left[\frac{3}{2}i - \frac{\chi_{\rm e}k^2}{n\omega} - \frac{3m_{\rm e}\nu_{\rm en}}{m_{\rm p}\omega}(1+\rho_{\rm en})\left(1+\frac{m_{\rm p}}{m_{\rm i}}N\right)\right]\bar{\tau}_{\rm e}, \quad (36)$$

where $g_{\rm en} = 1+\eta_{\rm e}k^2/\nu_{\rm en}(1+N)$.

The second equation relating $\bar{n}$ and $\bar{\tau}_{\rm e}$ can be obtained by eliminating $\boldsymbol{v}_{\rm e}$ and $\bar{\phi}_{\rm e}$ from the Euler equation for ions by means of equations (34) and (35). This yields

$$\bar{\tau}_{\rm e} = -\bar{n}\frac{T_{\rm i}}{T_{\rm e}}\left[\frac{c_s^2}{u_{T\rm i}^2} - i\frac{\nu^*_{\rm in}}{k^2u_{T\rm i}^2}\right.$$
$$\left.\times\left\{(1+\xi-i\Omega/\nu^*_{\rm in})\Omega + \frac{\omega}{\bar{\psi}g_{\rm en}}\right\}\right]. \quad (37)$$

Substitution of τ from equation (37) into equation (36) gives the dispersion equation. As in the case of the ion thermal instability, we consider only the relatively long-wavelength/low-frequency limit when $|\Omega|,\ kU_0,\ \eta k^2,\ \xi k^2/n \ll \nu^*_{\rm in}$. In this limit, we have the real part of frequency

$$\Omega_r = -\frac{\boldsymbol{k}\cdot\boldsymbol{U}_0}{1+(1+\xi)\bar{\psi}g_{\rm en}}. \quad (38)$$

Accounting for the terms that are second order in $|\Omega|/\nu^*_{\rm in}$ yields the following expression for the growth rate

$$\gamma = \frac{g_{\rm en}\bar{\psi}}{\nu^*_{\rm in}[1+(1+\xi)\bar{\psi}g_{\rm en}]}\left[\Omega_r^2 - k^2c_s^2 + \varepsilon\frac{m_{\rm p}\nu_{\rm pn}}{m_{\rm i}\omega_{\rm cp}}\right.$$
$$\left.\times\frac{1+N}{\frac{m_{\rm p}\chi k^2}{m_{\rm e}n\nu_{\rm en}}+3(1+\rho_{\rm en})\left(1+\frac{m_{\rm p}}{m_{\rm i}}N\right)}\frac{k^2U_0^2\sin2\theta}{1+(1+\xi)\bar{\psi}g_{\rm en}}\right]. \quad (39)$$

If the thermal conduction and viscosity effects can be ignored (conditions for this assumption as well as analysis of other characteristic length-scales in the chromosphere are presented in the next section), then equations (38) and (39) reduce to

$$\Omega_r = -\frac{\boldsymbol{k}\cdot\boldsymbol{U}_0}{1+\bar{\psi}}; \quad (40)$$

$$\gamma = \frac{\bar{\psi}}{\nu^*_{\rm in}(1+\bar{\psi})}\left[\frac{k^2U_0^2\cos^2\theta}{(1+\bar{\psi})^2} - \varepsilon^*\frac{(1+N)k^2U_0^2\sin2\theta}{3\kappa(m_{\rm i}/m_{\rm p}+N)(1+\bar{\psi})}\right.$$
$$\left. - k^2c_s^2\right], \quad (41)$$

where the effective heating coefficient $\varepsilon^* = \varepsilon/(1+\rho_{\rm en})$ represents the cumulative effect of two counter-acting processes: wave heating/collisional cooling.

Note that in the lower chromosphere, dominated by heavy ions, electron thermal effects are reduced (compared to the upper chromosphere) due to the presence of the $m_{\rm i}/m_{\rm p}$ ratio in the denominator of the second term on the right-hand side of equation (41). Analysis of equation (41) shows that the propagation angle θ_{ET} for the most unstable mode is given by

$$\tan2\theta_{ET} = \frac{2}{3}\varepsilon^*\frac{1+\bar{\psi}}{\kappa}\frac{1+N}{m_{\rm i}/m_{\rm p}+N}. \quad (42)$$

The threshold value of the current velocity is

$$U_{cr}^{ET} = c_s\sqrt{2}(1+\bar{\psi})$$
$$\times\left[1+\sqrt{1+\left(\frac{2}{3}\varepsilon^*\frac{1+\bar{\psi}}{\kappa}\frac{1+N}{m_{\rm i}/m_{\rm p}+N}\right)^2}\right]^{-1/2}. \quad (43)$$

Dependence of the threshold value of the current velocity U_0^{ET} on height in the chromosphere based on SRPM 306 is shown in Fig. 3 for $\varepsilon^* = 0$ (this case corresponds to FBI in the conditions of negligible ion magnetization), 1, 10, 30. The magnetic field $B =$ 30 G. The left-hand panel corresponds to the protons and the right to the ions with $m_{\rm i} = 30m_{\rm p}$.

From Fig. 3 one can see that, in the case of protons, the electron thermal effects cause a significant reduction of the threshold current velocity even for $\varepsilon^* = 1$, when there is no any plasma heating. For higher values of ε^*, the reduction of the threshold current velocity becomes very strong, and for $\varepsilon^* = 30$ the threshold value of the cross-field current velocity decreases about 10 times. However, our estimations, similar to those by Gogoberidze et al. (2009), show that this threshold reduction is insufficient to make the FBI heating comparable to the direct collisional heating by supercritical currents. It must be also noted that $U_{\rm cr}^{ET}$ is still much larger than the observed chromospheric currents (Socas-Navarro 2007).

In the case of heavy ions, the electron thermal effects are less important and for $\varepsilon^* = 1$ the influence of electron thermal effects on the FBI is negligible. But for higher values of ε^*, the decrease in U_0^{ET} becomes significant also in the case of heavy ions.

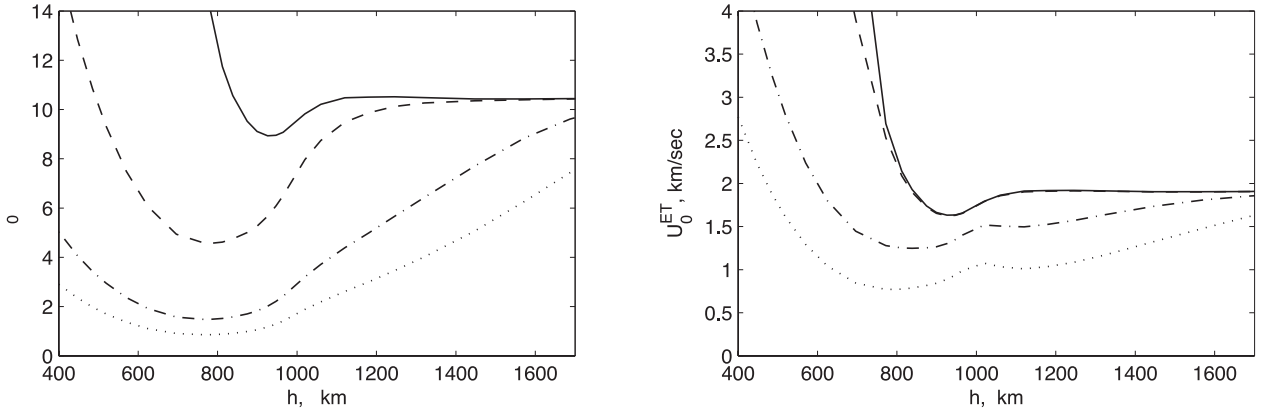

Figure 3. Dependence of the FBI threshold U_0^{ET} on the chromospheric height for $\varepsilon^* = 0$ (solid line), $\varepsilon^* = 1$ (dashed line), $\varepsilon^* = 10$ (das–dotted line) and $\varepsilon^* = 30$ (dotted line). Left-hand panel corresponds to the protons and right-hand panel to ions with $m_i = 30m_p$.

5 TYPICAL LENGTH-SCALES OF THE ELECTROSTATIC INSTABILITIES IN THE CHROMOSPHERE

In this section, we study in detail the assumptions made in the analysis presented above. We determine the typical length-scales of the electrostatic instabilities in the chromosphere. As mentioned in Section 2, perturbations of the neutral component can be ignored under the condition given in equation (15). The equivalent condition for the perturbation wavelength is

$$\lambda \ll \lambda_n \equiv \frac{2\pi c_s}{\nu_{in}} \frac{n_n}{n}. \tag{44}$$

The condition given in equation (16) that ion and electron thermal perturbations can be considered separately yields the condition for wavelength

$$\lambda \ll \lambda_T \equiv \frac{2\pi c_s}{\nu_{ep}} \frac{m_i}{m_e}. \tag{45}$$

In the derivation of equations (40)–(43), we ignored ion and electron viscosity and electron thermal conductivity effects. From equation (34), it follows that electron viscosity effects can be ignored if $\nu_{en} \gg \eta_e k^2$. Taking into account the expression for the electron viscosity (Braginskii 1965)

$$\eta_e = 0.73 \frac{\mathcal{K} T_e}{m_e \nu_{ep}}, \tag{46}$$

we find that the electron viscosity can be neglected under the following condition

$$\lambda \gg \lambda_e \equiv 2\pi \left(\frac{1+N}{0.73} \frac{\nu_{en}\nu_{ep}}{u_{Te}^2} \right)^{-1/2}. \tag{47}$$

According to equation (35), ion viscosity can be neglected if $\nu_{in}^* \gg \eta_i k^2$. Noting that the ion viscosity (Braginskii 1965)

$$\eta_i = 0.96 \frac{\mathcal{K} T_i}{\sqrt{m_e m_i}\nu_{ep}}, \tag{48}$$

we conclude that the ion viscosity can be neglected if

$$\lambda \gg \lambda_i \equiv 2\pi \left(\frac{\nu_{pn}\nu_{ep}}{0.96 u_{Tp}^2} \frac{m_e^{1/2}}{m_i^{1/2}} \right)^{-1/2}. \tag{49}$$

The perpendicular heat conductivity of electrons is (Braginskii 1965)

$$\chi_e = 4.66 \frac{n\mathcal{K} T_e \nu_{ep}}{m_e \omega_{ce}^2}. \tag{50}$$

Equation (36) yields that the electron heat conductivity can be neglected if

$$\lambda \gg \lambda_\kappa \equiv 2\pi \left[3 \left(\frac{1}{N} + \frac{m_p}{m_i} \right) \frac{\omega_{ce}\omega_{cp}}{4.66 u_{Te}^2} \right]^{-1/2}. \tag{51}$$

Finally, the long-wavelength approximation used to solve the dispersion equation is valid when

$$\lambda \gg \lambda_0 \equiv 2\pi \frac{c_s}{\nu_{in}^*}. \tag{52}$$

The characteristic wavelengths λ_n, λ_e, λ_i, λ_T, λ_κ and λ_0, as functions of chromospheric height based on SRPM 306 are presented in Fig. 4. The left-hand panel corresponds to protons and the right-hand panel to heavy ions with $m_i = 30m_p$. The magnetic field $B = 30$ G is assumed. Transition from the lower chromosphere with the effective ion mass $m_i \sim 30m_p$ to the upper chromosphere with $m_i \sim m_p$ occurs at the heights around 1000 km. This means the left-hand panel of Fig. 4 shows correct scales at $h > 1000$ km and the right-hand panel at $h < 1000$ km.

Assuming that the supercritical currents can occur in the solar chromosphere locally and generate FBI, from the right-hand panel of Fig. 4 we deduce that in the lower chromosphere, where the positively charged particles are mainly heavy ions, the typical FBI wavelengths are $\lambda = 10$–10^2 cm. In the upper chromosphere, where the positive charge is dominated by protons, the characteristic wavelengths are $\lambda = 10^2$–10^3 cm (see left-hand panel of Fig. 4). Since FBI generate plasma density perturbations, they can generate plasma irregularities with typical length-scales $\sim$10–10^2 cm in the lower and $\sim 10^2$–10^3 cm in the upper chromosphere. These plasma irregularities should cause scintillations of radio waves with similar wavelengths and provide a tool for remote chromospheric sensing. In particular, scintillations of decimetric/metric radio waves passing through solar chromosphere can serve as indicators for FBI developed in lower/upper chromosphere and hence for the presence of over-threshold currents there.

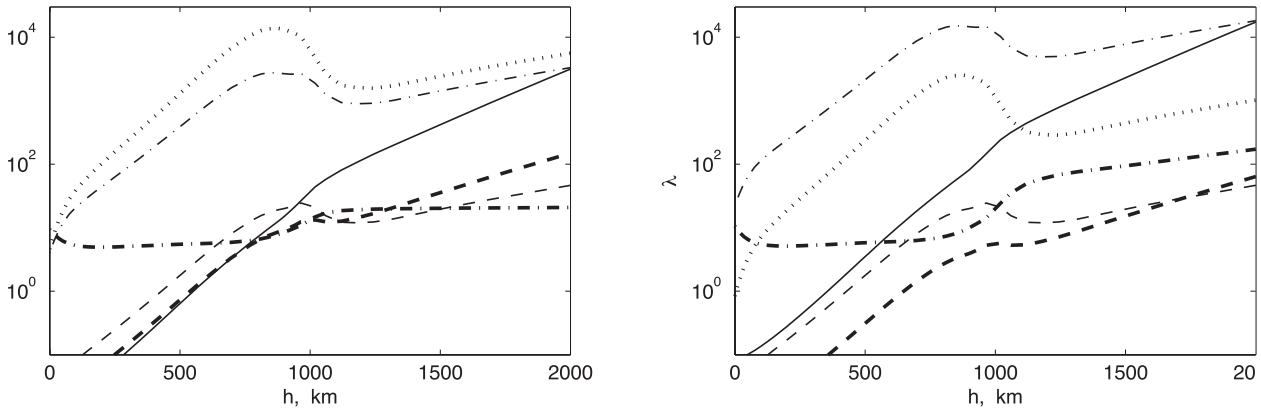

Figure 4. The characteristic FBI wavelengths as functions of the chromospheric height in the SRPM 306 model: λ_n (dotted line), λ_e (thin dashed line), λ_i (thick dashed line), λ_T (thin dash–dotted line), λ_κ (thick dash–dotted line) and λ_0 (solid line). Left-hand panel corresponds to the protons and right-hand panel to ions with $m_i = 30m_p$.

6 DISCUSSION

Since we are interested in more general features of FB-type instabilities, we do not analyse effects of inelastic electron–neutral collisions separately but incorporated them into the effective heating parameter $\varepsilon^* = \varepsilon/(1 + \rho_{en})$. This parameter reflects the response of electrons to the heating by waves (ε in the numerator) versus cooling by collisions ($1 + \rho_{en}$ in the denominator). Given the present uncertainty of both the heating factor ε and the inelastic collisional rates of electrons determining ρ_{en} in the chromosphere, the separate analysis of these effects is postponed for future considerations. A more detailed and justified model is also needed for the electron–neutral and ion–neutral collisions in the chromospheric conditions.

Several notes are in order regarding our study as compared to ionospheric studies. We would like to emphasize here two important facts concerning chromospheric plasma in contrast to ionospheric plasma: (i) Coulomb collisions (represented by N) cannot be ignored in the chromosphere and can increase the FBI growth rate; (ii) the ion/neutral mass ratio m_i/m_n is large in the middle/lower chromosphere, which leads to the decrease of the ion/neutral friction.

Since the Coulomb collisions usually introduce dissipative effects, their favourable influence on FBI is counter-intuitive and needs some explanation. As is known from ionospheric research (Oppenheim, Otani & Ronchi 1996; Schunk & Nagy 2000), the destabilizing term driving FBI is caused by the Pedersen response to the electric field perturbations, whereas the stabilizing term (proportional to $\kappa^2/(1 + N)$) is related to the Hall response. The intervention of Coulomb collisions in this picture is as follows: they abate the Pedersen term in the growth rate less than the Hall term and thus facilitate the FBI making it possible even for $\kappa > 1$.

Without effects introduced by the Coulomb collisions and large ion/neutral mass ratio (in the limit $N \to 0$ and $m_i/m_n \to 1$), our results are compatible with the results of ionospheric E-layer research. This conclusion follows from the comparison of our results on the thermal FBI effects with results by Dimant & Sudan (1995, 1997), Robinson (1998) and Dimant & Oppenheim (2004).

7 CONCLUSIONS

We investigated electrostatic instabilities of FB type in the partially ionized plasma of the solar chromosphere taking into account ion and electron thermal effects, electron and ion viscosity and Coulomb collisions. We derived the FBI growth rate including the ion thermal terms and found that the Coulomb collisions highly reduce them in the middle/upper chromosphere. Consequently, ion thermal effects can be neglected for FBI in the solar chromosphere.

In contrast, the electron thermal terms that contribute to the FBI growth rate (equation 41) are not negligible in the chromospheric conditions and cause a significant reduction of the threshold current triggering the instability. The ion and electron viscosity and thermal conductivity are also important and reduce the instability growth rate for relatively small-scale perturbations. We determined the characteristic length-scales relevant to chromospheric conditions as well as the threshold value of the current velocity as functions of height in the framework of the semi-empirical chromospheric model SRPM 306.

It has to be noted that the study of Gogoberidze et al. (2009) did not take into account the effect of additional electron heating related to the presence of parallel electric field in waves. As showed theoretically by Dimant & Milikh (2003) and confirmed by recent particle in cell simulations (Oppenheim & Dimant 2013), this effect can significantly increase the electron heating. Importance of this mechanism for the solar chromosphere requires separate analysis and is out of the scope of this paper.

In spite of the considerable threshold reduction by the electron thermal effects (see equation 43 and Fig. 3), our analysis showed that the electrostatic FB instabilities modified by the electron and ion thermal effects in chromospheric conditions are less efficient heating mechanisms than the collisional dissipation of cross-field currents that drive these instabilities. This conclusion concerns both the lower chromosphere, where the threshold velocity is decreased by heavy ions, and the middle/upper chromosphere, where the threshold velocity is decreased by the Coulomb collisions. As discussed in the introduction, our analysis ignored an additional electron heating related to the presence of parallel electric fields in waves. This effect is known to enhance significantly electron heating in the ionospheric E-layer, and therefore, we cannot exclude the possibility that similar effect can take place in the solar chromosphere as well. This subject require further investigations.

The characteristic wavelengths of the FB-type instabilities driven by supercritical currents in the solar chromosphere are $\lambda = 10$–10^3 cm. The plasma density fluctuations generated by these instabilities can produce scintillations of radio waves propagating through the chromosphere. The radio scintillations at $\sim$10 cm wavelengths are indicators for the FBI developed in the lower chromosphere, while the scintillations at $<10^3$ cm wavelengths suggest FBI in the

upper chromosphere. Observations and interpretations of such radio scintillations in terms of FBI provide a possibility for remote diagnostics of strong cross-field currents and plasma parameters in the solar chromosphere.

ACKNOWLEDGEMENTS

This research was supported by the Belgian Federal Science Policy Office (via IAP Programme – project P7/08 CHARM), by the European Commission's FP7 Programme (projects 263340 SWIFF, 313038 STORM, and SOLAIRE Network MTRN-CT-2006-035484), by FWO-Vlaanderen (project G.0304.07) and by K. U. Leuven (projects C90347 and GOA/2009-009).

REFERENCES

Aschwanden M. J., Tarbell T. D., Nightingale R. W., Schrijver C. J., Title A., Kankelborg C. C., Martens P., Warren H. P., 2000, ApJ, 535, 1047
Bedersen B., Kieffer L. J., 1971, Rev. Mod. Phys., 43, 601
Biermann L., 1946, Naturwissenschaften, 33, 118
Braginskii S. I., 1965, in Leontovich M. A., ed., Reviews of Plasma Physics. Consultants Bureau, New York, p. 205
Bruner E., 1978, ApJ, 226, 1140
Buneman O., 1963, Phys. Rev. Lett., 10, 285
Carlsson M., Stein R., 1992, ApJ, 397, L59
Dimant Ya. S., Milikh G. M., 2003, J. Geophys. Res., 108, 1350
Dimant Ya. S., Oppenheim M. M., 2004, J. Atm. Terr. Phys., 66, 1623
Dimant Ya. S., Sudan R. N., 1995, Phys. Plasmas, 2, 1169
Dimant Ya. S., Sudan R. N., 1997, J. Geophys. Res., 102, 2551
Farley D. T., 1963, J. Geophys. Res., 68, 6083
Fejer B. G., Providakes J., Farley D. T., 1984, J. Geophys. Res., 89, 7487
Fontenla J. M., 2005, A&A, 442, 1099
Fontenla J. M., Balasubramaniam K. S., Harder J., 2007, ApJ, 667, 1243
Fontenla J. M., Peterson W. K., Harder J., 2008, A&A, 480, 839
Fossum A., Carlsson M., 2005, Nature, 435, 919
Gogoberidze G., Voitenko Y., Poedts S., Goosens M., 2009, ApJ, 706, L12
Goodman M. L., 2004, A&A, 424, 691
Johnson L. C., 1972, ApJ, 174, 227
Krstic P. S., Schultz D. R., 1999, J. Phys. B: At. Mol. Opt. Phys., 32, 3485
Lighthill M. J., 1952, Proc. R. Soc. Lond. Ser. A, 211, 564
Liperovsky V. A., Meister C.-V., Liperovskaya E. V., Popov K. V., Senchenkov S. A., 2000, Astron. Nachr., 321, 129
Mein N., Schmieder B., 1981, A&A, 97, 310
Milikh G. M., Dimant Ya. S., 2003, J. Geophys. Res., 108, 1351
Oppenheim M., Dimant Ya. S., 2013, J. Geophys. Res., 118, 1306
Oppenheim M., Otani N., Ronchi C., 1996, J. Geophys. Res., 101, 17273
Pandey B. P., Wardle M., 2013, MNRAS, 431, 570
Parker E. N., 1988, ApJ, 330, 474
Rabin D., Moore R., 1984, ApJ, 285, 359
Robinson T. R., 1998, Adv. Space Res., 22, 1357
Schunk R. W., Nagy A. F., 2000, Ionospheres. Cambridge Univ. Press, Cambridge
Schwarzschild M., 1948, ApJ, 107, 1
Socas-Navarro H., 2007, ApJ, 633, L57
Stein R., 1967, Sol. Phys., 2, 385
Sturrock P. A., 1999, ApJ, 421, 451
Zaqarashvili T. V., Kukhianidze V., Khodachenko M. L., 2010, MNRAS, 404, L74

This paper has been typeset from a TEX/LATEX file prepared by the author.